AGU PUBLICATIONS

Global Biogeochemical Cycles

RESEARCH ARTICLE
10.1002/2013GB004743

Key Points:
- Global ocean carbon export is assessed using satellite observations
- Reproduces field observations and predicts sensible patterns in export efficiency
- Decadal-scale trends are found in global export efficiency

Supporting Information:
- Readme
- Figures S1–S4

Correspondence to:
D. A. Siegel,
davey@eri.ucsb.edu

Citation:
Siegel, D. A., K. O. Buesseler, S. C. Doney, S. F. Sailley, M. J. Behrenfeld, and P. W. Boyd (2014), Global assessment of ocean carbon export by combining satellite observations and food-web models, *Global Biogeochem. Cycles*, *28*, 181–196, doi:10.1002/2013GB004743.

Received 21 SEP 2013
Accepted 26 JAN 2014
Accepted article online 1 FEB 2014
Published online 10 MAR 2014

Global assessment of ocean carbon export by combining satellite observations and food-web models

D. A. Siegel[1], K. O. Buesseler[2], S. C. Doney[2], S. F. Sailley[3], M. J. Behrenfeld[4], and P. W. Boyd[5]

[1]Earth Research Institute and Department of Geography, University of California, Santa Barbara, California, USA, [2]Department of Marine Chemistry and Geochemistry, Woods Hole Oceanographic Institution, Woods Hole, Massachusetts, USA, [3]TMTF, Plymouth Marine Laboratory, Plymouth, UK, [4]Department of Botany and Plant Pathology, Oregon State University, Corvallis, Oregon, USA, [5]Institute for Marine and Antarctic Studies, University of Tasmania, Hobart, Tasmania, Australia

Abstract The export of organic carbon from the surface ocean by sinking particles is an important, yet highly uncertain, component of the global carbon cycle. Here we introduce a mechanistic assessment of the global ocean carbon export using satellite observations, including determinations of net primary production and the slope of the particle size spectrum, to drive a food-web model that estimates the production of sinking zooplankton feces and algal aggregates comprising the sinking particle flux at the base of the euphotic zone. The synthesis of observations and models reveals fundamentally different and ecologically consistent regional-scale patterns in export and export efficiency not found in previous global carbon export assessments. The model reproduces regional-scale particle export field observations and predicts a climatological mean global carbon export from the euphotic zone of ~6 Pg C yr^{-1}. Global export estimates show small variation (typically $< 10\%$) to factor of 2 changes in model parameter values. The model is also robust to the choices of the satellite data products used and enables interannual changes to be quantified. The present synthesis of observations and models provides a path for quantifying the ocean's biological pump.

1. Introduction

The oceans are a central component of the global carbon cycle through their storage, transport, and transformations of carbon constituents. In particular, ocean ecosystems control the biological pump which exports organic carbon from the well-lit, upper ocean, largely through the sinking of biogenic particles, into its stratified interior where it is sequestered on time scales ranging from seasons to centuries [e.g., *Falkowski et al.*, 1998; *DeVries et al.*, 2012]. Quantification of this carbon flux is critical for predicting the atmosphere's response to changing climate [*Bopp et al.*, 2001; *Kwon et al.*, 2009]. However, estimates of the global export flux remain highly uncertain, ranging from 5 to >12 Pg C yr^{-1} [*Boyd and Trull*, 2007; *Henson et al.*, 2011, hereinafter H11].

Present assessments of global export are made either by empirical extrapolations of field measurements to global scales using satellite-sensed estimates of export efficiency (the so-called e-ratio; often described as a function of sea surface temperature (SST)) and net primary production (NPP) [*Laws et al.*, 2000; *Dunne et al.*, 2005; H11] or by using global coupled carbon cycle-ocean circulation models [*Bopp et al.*, 2001; *Gehlen et al.*, 2006; *Doney et al.*, 2009]. Yet estimates of global export remain widely divergent (5 to >12 Pg C yr^{-1}) with a range as large as the present annual anthropogenic CO_2 emission rate.

Sinking particles are ultimately created by the photosynthetic production of organic matter in the euphotic zone, whose depth is usually defined as the depth at which 1% of the flux of incident photosynthetically available radiation (PAR) is found. Fixed organic carbon in the euphotic zone is subsequently transformed by community respiration, particle aggregation, zooplankton grazing and feces production, and microbial decomposition processes. These processes all contribute to the proportion of fixed organic carbon that is exported from the upper ocean [e.g., *Michaels and Silver*, 1988; *Aksnes and Wassmann*, 1993; *Boyd and Trull*, 2007; *Buesseler and Boyd*, 2009].

Mechanistically, it is the flux of sinking carbon leaving the euphotic zone that is relevant; yet most measurements of export flux are made at a fixed depth horizon because sampling at the base of the euphotic zone with conventional sediment traps is difficult [e.g., *Boyd and Newton*, 1997; *Buesseler and Boyd*, 2009]. This makes the comparison of export flux determinations problematic. If the sampling horizon is too deep, the export flux may be rapidly attenuated within the mesopelagic, whereas if the sampling horizon is within the

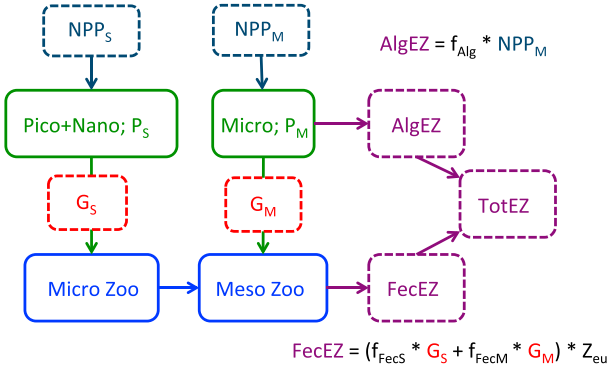

Figure 1. Diagram of the pelagic food web supporting the flux of sinking particles from the euphotic zone (TotEZ). TotEZ is comprised of the flux of sinking intact algal cells (AlgEZ) and the flux of fecal matter from large zooplankton (FecEZ), and they are shown in violet in the diagram. Stocks of phytoplankton are shown in solid green lines and for zooplankton in blue lines. The grazing and NPP fluxes that regulate the stocks are shown in dashed lines and the assumed parameterizations for FecEZ and AlgEZ are given.

euphotic zone, much of the flux may be missed [e.g., *Buesseler et al.*, 2007; *Buesseler and Boyd*, 2009; *Burd et al.*, 2010]. Euphotic zone depths vary from ~20 m to more than 120 m regionally and with season (see below), and global studies of carbon export must account for these changes [*Buesseler and Boyd*, 2009].

The sinking particle flux is often modeled as the sum of the flux of fecal matter from zooplankton grazing and the flux from sinking algal cells and associated aggregates [e.g., *Michaels and Silver*, 1988; *Buesseler and Boyd*, 2009]. Observations of high direct algal fluxes are typically associated with blooms of large phytoplankton [e.g., *Billett et al.*, 1983; *Boyd and Stevens*, 2002], while elevated levels of fecal export fluxes are associated with elevated zooplankton activity [e.g., *Michaels and Silver*, 1988; *Aksnes and Wassmann*, 1993]. Since large phytoplankton are grazed by large zooplankton that have significant contribution to export (i.e., fecal pellets), the larger the phytoplankton, the more efficiently euphotic zone NPP is partitioned into export.

Here we introduce a novel, satellite-based approach for assessing global carbon export that accounts for the food-web processes that create sinking particulate matter. We employ recent advances in satellite remote-sensing methodologies that: (1) quantify rates of net primary production based upon optical estimates of phytoplankton carbon biomass [*Behrenfeld et al.*, 2005; *Westberry et al.*, 2008]; (2) assess the slope of the particle size spectrum enabling NPP and phytoplankton carbon biomass to be partitioned by size class [*Kostadinov et al.*, 2009, 2010]; and (3) estimate rates of zooplankton grazing on phytoplankton from upper-ocean phytoplankton carbon biomass budgets [*Behrenfeld*, 2010; *Behrenfeld et al.*, 2013]. Combining these components, a mechanistic, yet simple, model for the sinking carbon export from the euphotic zone (TotEZ) can be created. The resulting model reproduces regional-scale export field observations and its global summaries are robust to large changes in model parameters or the exact data products used. Importantly, the retrieved export efficiency patterns reflect an ecological realism not found in previous remote-sensing-based assessments.

2. Food-Web Modeling

The method presented is meant to be a first step toward quantifying global carbon export due to sinking particles from the euphotic zone (TotEZ) through synthesizing satellite observations and food-web models (Figure 1). Our aim is to match model complexity with the present state of satellite data products and to identify directions for improvements. The food web assumes that large (micro-) and small (pico- and nano-) phytoplankton are grazed by large (meso-) and small (micro-) zooplankton, respectively (Figure 1). The total flux of sinking particles from the euphotic zone (TotEZ) is modeled as the sum of the flux of sinking algal cells and associated aggregates (AlgEZ) and the flux of fecal matter from zooplankton grazing (FecEZ), or

$$\mathrm{TotEZ} = \mathrm{AlgEZ} + \mathrm{FecEZ}. \quad (1)$$

All three terms are in units of mg C m^{-2} d^{-1}. This partitioning of export follows many food-web and interdisciplinary ocean system models [e.g., *Michaels and Silver*, 1988; *Boyd and Stevens*, 2002; *Aumont and Bopp*, 2006; *Buesseler and Boyd*, 2009]. The food-web relationships from Figure 1 illustrate that some of the primary production energy in large phytoplankton (P_M) is lost from the euphotic zone on sinking particles (AlgEZ), while the grazing of P_M by large zooplankton (G_M) contributes to fecal export (FecEZ). Similarly, small phytoplankton biomass (P_S) is consumed by smaller zooplankton (G_S), which in turn is consumed by large zooplankton that contribute to FecEZ (Figure 1).

Direct algal export, AlgEZ, is comprised only by large phytoplankton and is modeled as a linear function of the net primary production of large phytoplankton (NPP_M), or

$$\mathrm{AlgEZ} = f_{\mathrm{Alg}}\mathrm{NPP_M} \tag{2}$$

where the parameter f_{Alg} quantifies the transformation efficiency of microphytoplankton NPP, NPP_M, that sinks from the euphotic zone, where NPP is the vertically integrated net primary production over the euphotic zone. Values of NPP_M are calculated from remote-sensing estimates of NPP and the proportion of microphytoplankton biovolume (F_M) as described in section 3 below. A value of 0.1 is used for f_{Alg} in our baseline case, consistent with energy transfer efficiencies chosen in previous food-web models [e.g., *Michaels and Silver*, 1988; *Boyd and Stevens*, 2002; *Boyd et al*., 2008]. Logically, the value for f_{Alg} cannot be much larger than 10% because NPP energy inputs to large phytoplankton are also balanced by population growth, zooplankton grazing, viral lysis, dissolved organic carbon (DOC) release and direct sinking losses (AlgEZ). Implications of this and other parameter choices are addressed below.

The fecal export flux (FecEZ) is modeled as fixed fractions of the zooplankton grazing rate on large (G_M) and small (G_S) phytoplankton averaged over the euphotic zone (Z_{eu}), or

$$\mathrm{FecEZ} = \left(f_{\mathrm{FecM}}G_{\mathrm{M}} + f_{\mathrm{FecS}}G_{\mathrm{S}}\right) Z_{\mathrm{eu}} \tag{3}$$

where f_{FecM} and f_{FecS} quantify the fraction of grazing on microphytoplankton and small phytoplankton that contributes to the fecal sinking flux leaving the euphotic zone. Assumed values for f_{FecM} and f_{FecS} are 0.3 and 0.1, respectively, following parameterizations used in recent ocean ecosystem models [*Aumont and Bopp*, 2006; *Doney et al*., 2009] and consistent with previous food-web modeling studies [*Michaels and Silver*, 1988; *Boyd and Stevens*, 2002; *Boyd et al*., 2008]. The smaller value of f_{FecS} compared with f_{FecM} accounts for the two trophic steps between grazing on small phytoplankton and the production of FecEZ by large zooplankton (Figure 1).

Grazing mortalities for the two size classes (G_M and G_S) are diagnosed from the mass budget of mixed layer phytoplankton carbon concentration. The time rate of change of biomass for microphytoplankton (P_M) and small phytoplankton (P_S) in the surface mixed layer can be expressed as

$$\frac{\mathrm{d}P_i}{\mathrm{d}t} = \frac{\mathrm{NPP}_i}{Z_{\mathrm{eu}}} - G_i - m_{\mathrm{ph}}P_i - \delta_{i,\mathrm{M}}\frac{\mathrm{A1gEZ}}{Z_{\mathrm{eu}}} - \mathrm{Detrn}(Z_{\mathrm{ml}}, P_i), \tag{4}$$

where NPP_i is the net primary production rate for size class i (mg C m^{-2} d^{-1}), G_i is its grazing mortality (mg C m^{-3} d^{-1}), Z_{ml} is the mixed layer depth, m_{ph} is the nongrazing phytoplankton specific mortality rate, AlgEZ is the flux of large phytoplankton biomass from the euphotic zone (equation (2) and $\delta_{i,M} = 1$ when $i = M$ and 0 otherwise), and Detrn(Z_{ml},P_i) represents the entrainment-driven reduction in phytoplankton biomass as the mixed layer deepens. The nongrazing, phytoplankton specific mortality is set equal to 0.1 day^{-1} following values chosen for existing global ecosystem coupled models [e.g., *Aumont and Bopp*, 2006; *Doney et al*., 2009]. Following *Evans and Parslow* [1985], the detrainment loss rate of phytoplankton carbon from the mixed layer can be modeled as

$$\frac{\mathrm{d}P_i}{\mathrm{d}t} = \frac{\mathrm{NPP}_i}{Z_{\mathrm{eu}}} - G_i - m_{\mathrm{ph}}P_i - \delta_{i,\mathrm{M}}\frac{\mathrm{A1gEZ}}{Z_{\mathrm{eu}}} - \frac{P_i}{Z_{\mathrm{ml}}}\frac{\mathrm{d}Z_{\mathrm{ml}}}{\mathrm{d}t}H\left(\frac{\mathrm{d}Z_{\mathrm{ml}}}{\mathrm{d}t}\right) \tag{5}$$

where $H(x) = 1$ if $x > 0$ and 0 otherwise.

There are several important assumptions made here. It is assumed that satellite estimates of biomass (P_i) and NPP are uniform over the mixed layer and that the impacts of AlgEZ on P_i losses from the euphotic zone are uniform over Z_{ml}. Further, we assume that P_i concentrations below Z_{ml} are negligible. This means that the dilution in biomass concentrations in the mixed layer during mixed layer deepening ($dZ_{ml}/dt > 0$) are accounted for by the detrainment parameterization, and the nonentrainment diffusive fluxes are small. Last, we assume that the value of m_{ph}, the phytoplankton specific mortality (day^{-1}) due to biological losses not leading to export, is the same for microphytoplankton and small phytoplankton. Given the above assumptions, the grazing mortality for each phytoplankton size class, G_i, can be diagnosed from satellite and available data by rearranging equation (5). Together with estimates of NPP_M and Z_{eu}, TotEZ can be derived using equations (1) to (3). The fraction of NPP that is exported from the euphotic zone provides a useful

metric for export efficiency (EZ-Ratio = TotEZ/NPP), while the ratio of AlgEZ to TotEZ quantifies the importance of the export of algal materials to export.

3. Data and Methods

3.1. Data Sources

The analyses presented here are for a climatological year constructed largely from observations made by the Sea-viewing Wide-Field-of-view Sensor (SeaWiFS) satellite ocean color mission [*McClain*, 2009; *Siegel et al*., 2013]. While the SeaWiFS mission spanned from October 1997 to November 2010, temporal export estimates presented here were restricted to the end of December 2008 due to sampling issues later in the mission.

Phytoplankton carbon biomass (P_T) is modeled using retrievals of the particulate backscattering coefficient at 443 nm (BBP) [*Behrenfeld et al*., 2005; *Westberry et al*., 2008; *Siegel et al*., 2013]. BBP fields from SeaWiFS imagery are available at http://wiki.eri.ucsb.edu/measures/index.php/GSM. In testing model sensitivity, an alternative estimate of phytoplankton biomass is created using the SeaWiFS-measured chlorophyll concentration and a fixed carbon to chlorophyll ratio of 50.

Values of NPP come from version 2 of the Carbon-based Productivity Model (CbPMv2) [*Westberry et al*., 2008] using data from the SeaWiFS mission. The CbPMv2 relates NPP to the product of phytoplankton carbon biomass (as described above) and the phytoplankton specific growth rate, modeled from the satellite-measured chlorophyll to carbon ratio and the mixed layer growth irradiance [*Behrenfeld et al*., 2005; *Westberry et al*., 2008]. Data fields for the CbPMv2 are available at http://www.science.oregonstate.edu/ocean.productivity/carbon2.model.php. The Vertically Generalized Production Model (VGPM) [*Behrenfeld and Falkowski*, 1997] is also used in testing model sensitivity and these data are available at http://www.science.oregonstate.edu/ocean.productivity/onlineVgpmData.php.

The fraction of total phytoplankton carbon biomass in the microphytoplankton size range, F_M, is modeled from the slope of the particle size distribution (PSD) retrieved from SeaWiFS reflectance observations [*Kostadinov et al*., 2009, 2010]. The approach uses Mie modeling to relate the SeaWiFS-measured slope of the particulate backscattering spectrum to a linear PSD slope [*Kostadinov et al*., 2009]. The fraction of the total particle biovolume ($D_{min} > D \geq D_{max}$; 0.5 μm $> D \geq$ 50 μm) in the microphytoplankton size range ($D_{spl} > D \geq D_{max}$; 20 μm $> D \geq$ 50 μm) is calculated following procedures in *Kostadinov et al*. [2010]. We assume that the fraction of phytoplankton biomass and NPP in the two different size classes is proportional to the biovolume (particle volume per seawater volume) in each size class. Hence, $P_M = F_M * P_T$ and $P_S = (1 - F_M) * P_T$, and a similar partitioning is performed for NPP. Data fields for the slope of the particle size distribution are available at http://wiki.icess.ucsb.edu/measures/index.php/PSD.

The depth of the euphotic zone, Z_{eu}, is modeled as the depth where 1% of the surface PAR is found. Values of surface chlorophyll concentration from SeaWiFS are used to estimate Z_{eu} following algorithms presented in *Morel et al*. [2007]. SeaWiFS chlorophyll *a* concentrations are taken from the NASA ocean color website http://oceancolor.gsfc.nasa.gov/cgi/l3?sen=S&per=MO&prod=CHL_chlor_a.

Mixed layer depth, Z_{ml}, values are taken from the MLD_DT02 climatology [*de Boyer Montégut et al*., 2004]. Monthly climatology for Z_{ml} values is available from http://www.ifremer.fr/cerweb/deboyer/mld/Surface_Mixed_Layer_Depth.php. The MLD_DT02 climatology determines Z_{ml} from more than 5 million vertical temperature profiles as the depth at which temperature is less than 0.2°C from the value at 10 m. Time varying fields of Z_{ml} are taken from those used in the CbPMv2 modeling (see http://www.science.oregonstate.edu/ocean.productivity/inputData.php for details).

3.2. Calculation Details

All data are regridded onto a 1° latitude/longitude grid and averaged for each climatological month. A grid location is used if data from all of the different sources are available for at least 8 months of the year. Monthly observations are then spline fit to create a monthly time series. Integration of the modeled spatial fields to assess global statistics is made after cosine weighting each 1° bin by its latitude. The resulting area of the ocean considered is 3.16×10^8 km^2, which includes nearly all of the ocean equatorward of 65° latitude. The area considered is about 20% smaller than the total area of ocean (3.61×10^8 km^2). Regions that do not meet

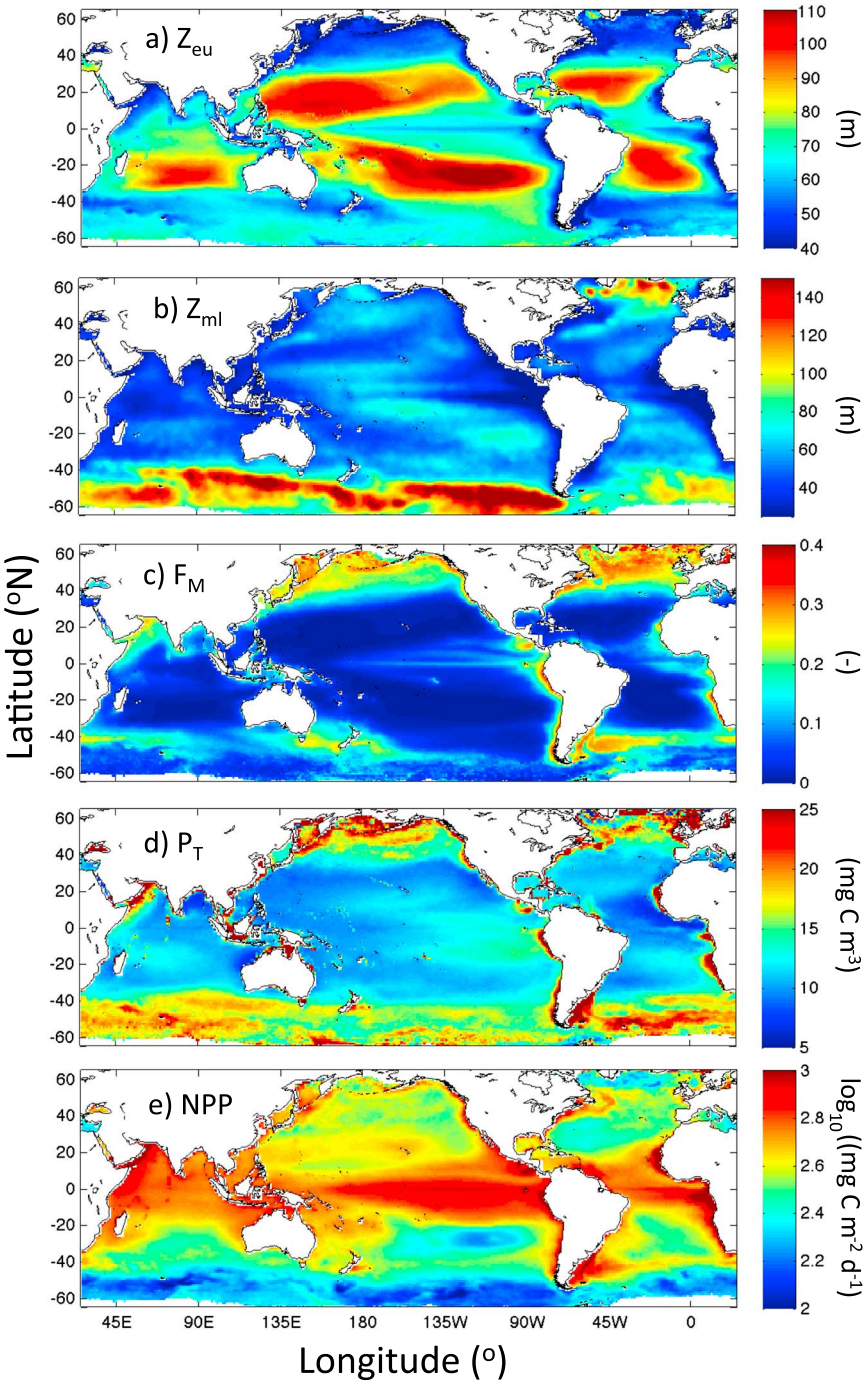

Figure 2. Time mean distributions of (a) the euphotic zone depth (Z_{eu}), (b) the mixed layer depth (Z_{ml}), (c) the fraction of biomass in the microphytoplankton size class (F_M), (d) the total phytoplankton biomass (P_T), and (e) the net primary production (NPP). Data are averaged over the period October 1997 to October 2008.

our selection criteria are mostly in high-latitude ocean due largely to seasonally low Sun elevations and persistent cloud and ice cover.

3.3. Field Validation

Measurements of the radioactive activity of the short-lived, particle-reactive isotope ^{234}Th ($\tau_{½}$ = 24.1 day) are most often depleted in surface seawater relative to the activity of its conservative and long-lived parent, ^{238}U.

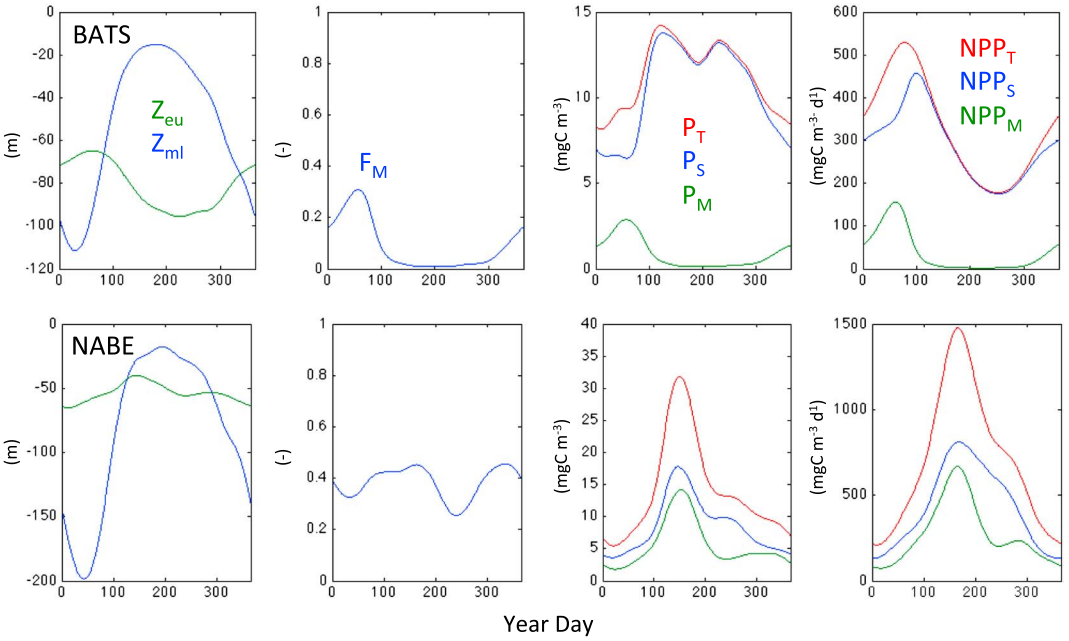

Figure 3. Time series of input data sets from the location of (top) the Bermuda Atlantic Time series Site (BATS; 32°N 64°W) and (bottom) the North Atlantic Bloom Experiment (NABE; 47°N 20°W; bottom). From left to right, the panels illustrate (first column) the climatological variations in Z_{eu} (green) and Z_{ml} (blue), (second column) the fraction of biomass in the microphytoplankton size class, F_M, (third column) the total phytoplankton (P_T; red), small phytoplankton (P_S; blue), and the microphytoplankton (P_M; green) biomass, and (fourth column) the total and size-fractionated NPP. Figure S1 shows the time variations of the same quantities at the other time series locations used in the model validation.

Sinking particles drive the ^{234}Th:^{238}U deficit, which is now measured routinely as a tracer for particle export from the upper ocean [*Rutgers van der Loeff et al.*, 2006; *Waples et al.*, 2006]. POC export is quantified by multiplying the ^{234}Th flux (calculated from ^{234}Th measurements in the water column) by the POC:^{234}Th ratio on sinking particles [*Buesseler et al.*, 2006]. An advantage of the ^{234}Th method is that water column profiles of ^{234}Th deficits can be used to estimate POC fluxes at specific depths including Z_{eu}.

We use *Buesseler and Boyd*'s [2009] recent summary of ^{234}Th derived POC fluxes at the base of the euphotic zone as the basis of our validation data set. These observations represent a wide range of production, sinking carbon flux, and export efficiencies and considerable background information is available (supporting information Table S1 provides a listing of the sites, their locations, and citations to the fundamental studies). An additional sampling of the North Atlantic Bloom Experiment (NABE) site in the summer was added (NABE July) [*Lampitt et al.*, 2008] to emphasize the seasonal variability in the observations and models. An analysis of POC export from the Bermuda Atlantic Time series Site (BATS) is also included, calculated as the annual average of 150 m sediment trap data from 1990 to 2006 [*Steinberg et al.*, 2001] and extrapolated to 100 m, near the climatological mean euphotic zone depth [*Siegel et al.*, 2001], using the long-term mean difference between the 150 and 200 m depth trap fluxes. A few high-latitude sites from the *Buesseler and Boyd* [2009] study were not included as satellite observations were not available for the 8 months required. The field determinations and the climatological model calculations do not represent the same time periods, and a matchup of field observations is not possible because many of the field observations were made before SeaWiFS was launched.

4. Results

4.1. Distributions of Input Data

Climatological mean distributions of Z_{eu} and Z_{ml} are shown in Figures 2a and 2b, respectively. Deep mean values of Z_{eu} (≥100 m) are found in the subtropical oceans while shallow values (≤ 50 m) are found in the subarctic seas and near-continental boundaries illustrating the importance of quantifying the carbon export from the euphotic zone rather than a fixed depth horizon. Mean values of Z_{ml} have nearly an opposite pattern compared with Z_{eu} with shallow mean Z_{ml} values in the subtropical oceans and higher values in the subarctic

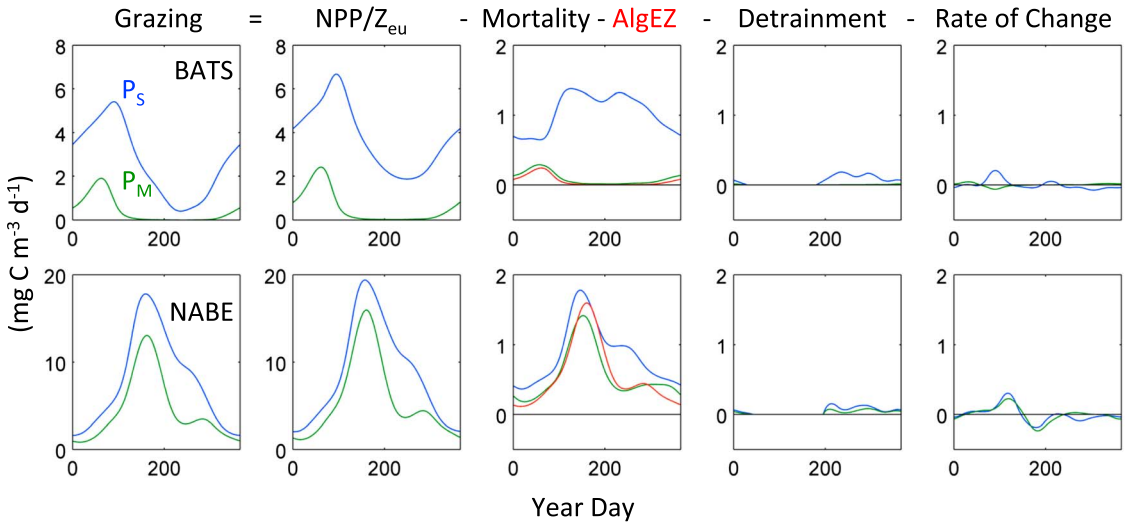

Figure 4. Calculation of grazing rates from climatological time series observations from the (top) BATS and (bottom) NABE locations. The green curves show the microphytoplankton biomass budget (P_M) while the blue curves illustrate the changes to small phytoplantkon (P_S). The panels are ordered from left to right illustrating (first panel) the contribution that each process makes to the grazing rates (G_M and G_S in mg C m^{-3} d^{-1}). The second panel shows the NPP rates for the two size classes. The third panel shows the time series of nongrazing biological losses for the two size classes and the direct loss of large phytoplankton from the mixed layer (AlgEZ/Z_{eu}; shown in red). The fourth panel shows the detrainment losses of P_M and P_S, and the fifth panel shows the time rate of change of P_M and P_S. Note the change of vertical scales in the different panels and the general decrease in rates (all in mg C m^{-3} d^{-1}) from left to right. Examples for other locations are provided in supporting information Figure S2.

(Figure 2b). Time series of Z_{ml} from the BATS and NABE locations show the expected patterns of deep winter mixed layers and shallow summer Z_{ml} values (Figure 3). Euphotic zone depths vary from about 60 m to nearly 100 m at BATS and from roughly 40 m to 60 m at NABE.

The mean spatial distribution for the fraction of microphytoplankton size biovolumes, F_M, is shown in Figure 2c, and its seasonal variability at the BATS and NABE locations is presented in Figure 3. Mean values of F_M vary from near zero in the subtropical gyres to greater than 40% in the subarctic oceans. The microphytoplankton biovolume fraction is also greater in eastern boundary current and equatorial upwelling regions where vertical upwelling processes create higher rates of NPP. Time variability at BATS shows a strong spring bloom where F_M values approach 40% in the early spring whereas values at NABE remain near 35% throughout the seasonal cycle (Figure 3).

The climatological mean distribution of phytoplankton carbon biomass estimated from satellite observations (P_T) is shown in Figure 2d, and its seasonal variations at BATS and NABE are shown in Figure 3. Values of P_T are lower in the subtropical gyres and the tropics (~5 to 15 mg C m^{-3}) and are greater than 20 mg C m^{-3} in the subarctic oceans and eastern boundary current regions. The time variability of P_T at BATS shows higher values of P_T in the summer after the spring bloom, while a strong increase in P_T is found in June at NABE corresponding to the spring bloom there.

Spatial mean distribution of log-transformed NPP estimated from the CbPMv2 algorithm is shown in Figure 2e and its seasonal variations at the BATS and NABE time series locations are shown in Figure 3. As expected, values of NPP are elevated (approaching 1 g C m^{-2} d^{-1}) throughout the tropics and for regions where persistent nutrient inputs are found. NPP estimates vary over time by more than a factor of 2 for both the BATS and NABE locations (Figure 3).

4.2. Estimation of Grazing Rates and TotEZ

Grazing rates on large (G_M) and small (G_S) phytoplankton are derived from the mixed layer phytoplankton biomass budget (equation (5)). Figure 4 displays the contributions of the terms in equation (5) to the estimates of G_M and G_S grazing mortalities for the annual cycle at BATS and NABE. Grazing rates are nearly equal to NPP$_i$/Z_{eu} illustrating the tight connection between phytoplankton production and zooplankton-mediated losses [e.g., *Banse*, 1992, 2013; *Behrenfeld et al.*, 2013]. Contributions from the other terms in equation (5) are all considerably smaller, although rarely the nongrazing losses of P_S can approach the value of NPP$_S$/Z_{eu} (e.g., summer at BATS) (Figure 4).

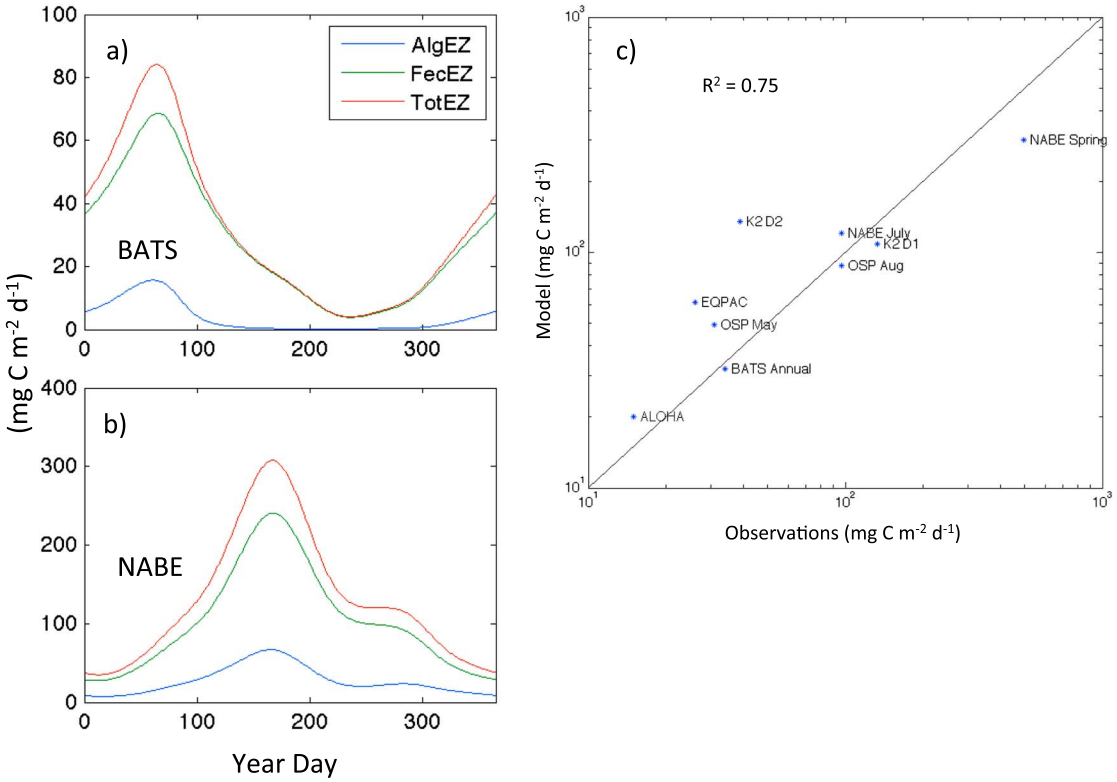

Figure 5. Time series of TotEZ (red), FecEZ (green), and AlgEZ(blue) fluxes (in mg C m^{-2} d^{-1}) for the (a) BATS and (b) NABE locations. (c) Comparison of field and modeled TotEZ estimates using the ^{234}Th disequilibrium method to estimate TotEZ from water column profile observations. Locations of the TotEZ field estimates are given in supporting information Table S1 and time series of export from these locations is presented in Figure S3.

Determinations of AlgEZ, FecEZ, and TotEZ are shown for the BATS and NABE sites in Figures 5a and 5b, respectively. A fourfold difference in total export is seen between the two sites while strong seasonal cycles are found at both sites in correspondence with observations [*Steinberg et al.*, 2001; *Lampitt et al.*, 2010]. The NABE site is also more efficient in converting NPP into sinking C flux and annual average EZ-ratio estimates are 8.4% and 18.1% for the BATS and NABE sites, respectively. Values of TotEZ are dominated by FecEZ at both sites; however, the mean contribution of algal export is greater at NABE than at BATS (annual mean AlgEZ/TotEZ are 8.2% and 21.0% for BATS and NABE, respectively).

The correspondence between the modeled and observed TotEZ values is striking, as paired determinations straddle the one-to-one line (Figure 5c). The linear regression coefficient between the two log-transformed export estimates explains 75% of the variance. This result is excellent considering that we are comparing field observations with a modeled climatology. The differences in time periods likely explain some of the mismatches found between climatological model and field observations.

4.3. Global Patterns of TotEZ and EZ-Ratio

The global distribution of annual mean, log-transformed TotEZ is shown in Figure 6a. Spatial patterns illustrate elevated values of TotEZ in the tropical and subpolar oceans while lower values are observed in the subtropical gyres. The TotEZ distribution approximates a log-normal distribution illustrating the importance of a few sites with high TotEZ to global integrals (Figure 7a). The model with its baseline parameters predicts 5.7 Pg C annually exported from the euphotic zone summed over all ocean regions where satellite data are available (equatorward of 65° latitude).

Spatial patterns of the annual average EZ-ratio, defined as TotEZ/NPP (Figure 6c), show expected oceanographic features with lower values (≤0.05) in the subtropical gyres and higher values (>0.15) for regions where larger phytoplankton dominate pelagic food webs (compare with Figure 2c). The global mean EZ-ratio is 10.3% with a standard deviation (SD) of 5.0%. Very few values of the modeled climatological mean EZ-ratio are greater than 20% (Figure 7b).

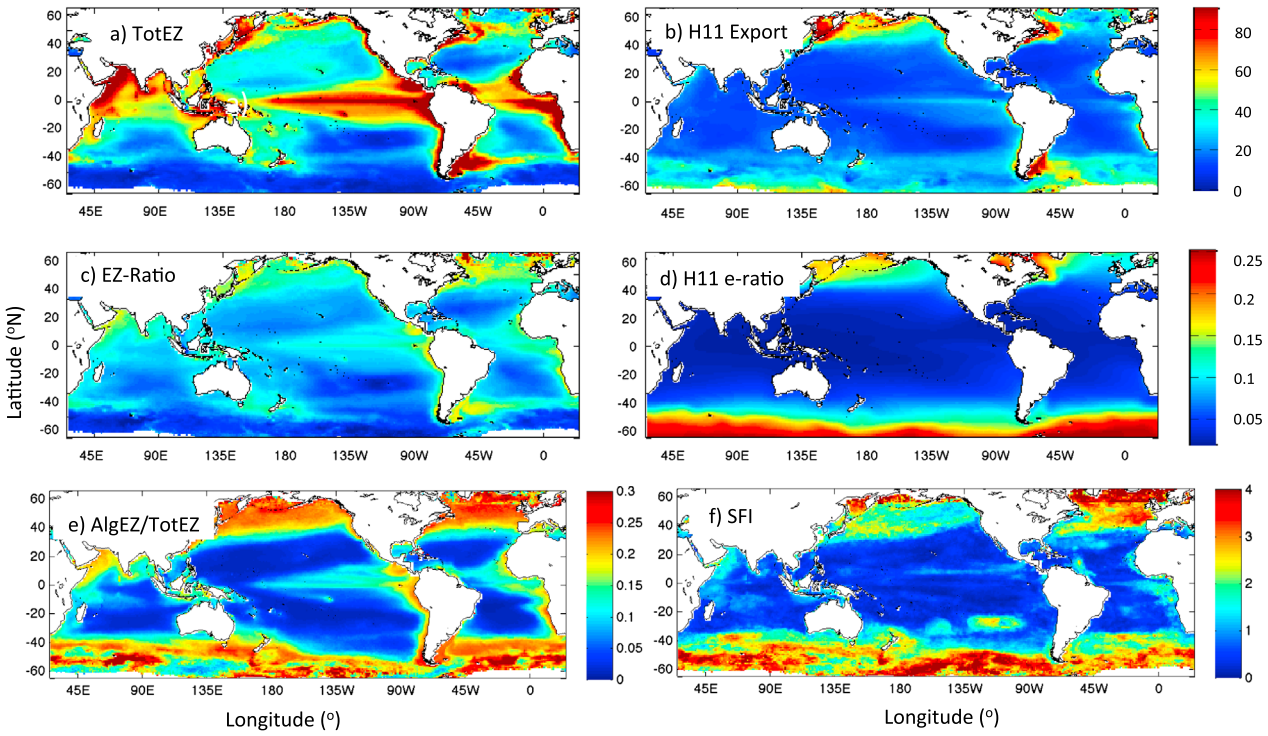

Figure 6. Global distributions of the annual mean (a) $\log_{10}$(TotEZ) (mg C m^{-2} d^{-1}), (b) $\log_{10}$-transormed export flux at 100 m calculated using the H11 e-ratio (mg C m^{-2} d^{-1}), (c) the ratio of TotEZ to NPP, EZ-ratio (unitless), (d) the H11 e-ratio (unitless), (e) ratio of AlgEz to TotEZ (unitless), and (f) seasonal flux index (SFI; unitless).

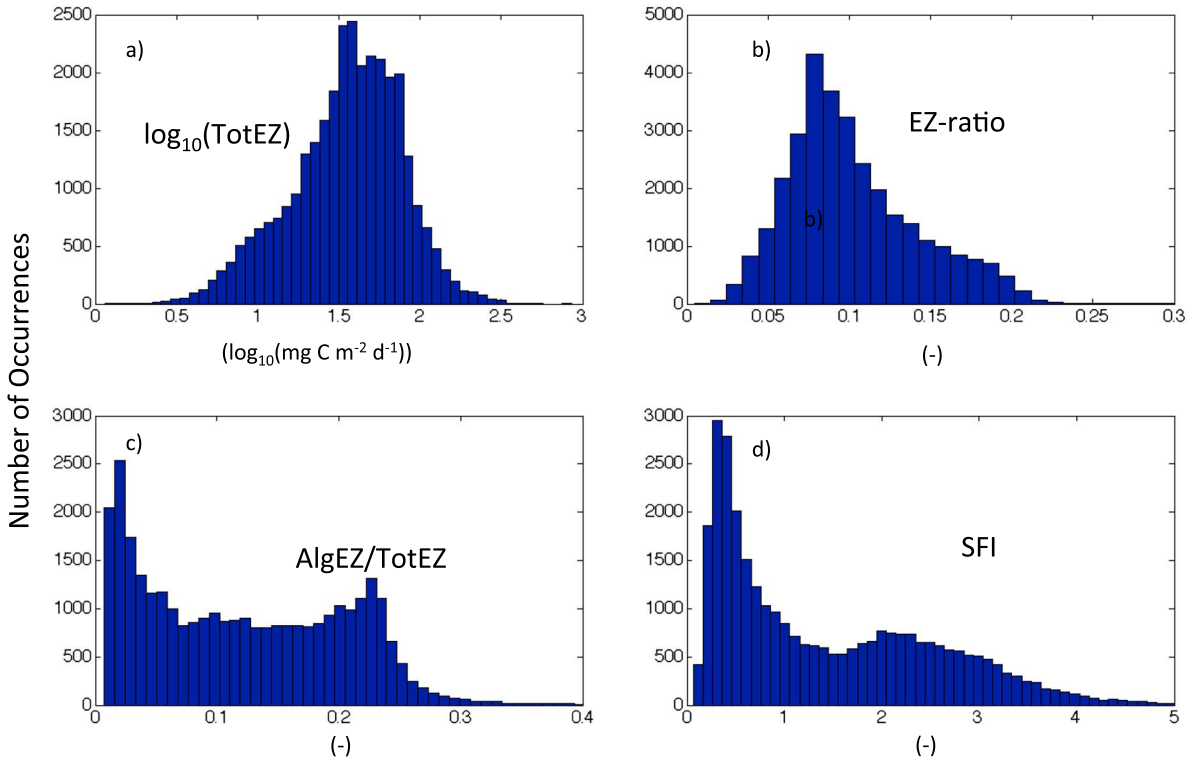

Figure 7. Probability density functions for annual mean (a) TotEZ, (b) EZ-ratio, (c) AlgEz/TotEZ, and (d) the seasonal flux index (SFI). The SFI is defined as the difference between the monthly maximum and the monthly minimum TotEZ normalized by the annual mean TotEZ.

The present approach shows improved realism compared with previous empirical models of global export flux and its efficiency. For example, *Henson et al*. [2011] performed a regression analysis of available ^{234}Th, NPP, and SST observations to create an empirical model for the export efficiency factor (e-ratio) at 100 m. Spatial patterns of the H11-modeled export flux and the e-ratio at 100 m are shown in Figures 6b and 6d, respectively. The spatial pattern for the H11 e-ratio simply reflects the assumed inverse relationship with SST with higher values toward the poles and lower values in the tropics. The H11-parameterized e-ratio spatial pattern (Figure 6d) does not look like the present EZ-ratio spatial distribution (Figure 6c) nor does it share the basic spatial patterns with NPP (Figure 2e), phytoplankton carbon (Figure 2d), or microphytoplankton biovolume fraction (Figure 2c).

The H11-parameterized particle export values at 100 m show muted variations compared with the present TotEZ estimates (compare Figures 6a and 6b). The globally integrated export at 100 m from the H11 parameterization is 3.4 Pg C yr^{-1}, far smaller than the 5.7 Pg C yr^{-1} found with the present approach using the same NPP algorithm (CbPMv2) and domain. Although larger in magnitude, similar results are found using the *Laws et al*. [2000] parameterization for export efficiency, as it too parameterizes the e-ratio as a decreasing function of SST. In all, the present determinations of TotEZ and the EZ-ratio differ substantially from previous approaches illustrating spatial patterns consistent with the assumed ecological processes driving export.

The ratio of AlgEZ/TotEZ quantifies the relative contribution made by the direct sinking of algal cells. The global mean value of AlgEZ/TotEZ is 12.7% (5.7% SD) and its mean spatial patterns are shown in Figure 6e. High contributions of AlgEZ to total export (≥ 20%) are found in the high-latitude oceans and upwelling regions where larger phytoplankton sizes predominate (Figure 2c). Only rarely are values of AlgEZ/TotEZ found greater than 25% (Figure 7c).

The current model effectively captures the strong seasonal cycles that occur in carbon export [e.g., *Lutz et al*., 2007], and the modeled TotEZ flux time series vary dramatically over the seasonal cycle (Figures 5a, 5b, and S3). The difference between the maximum and minimum modeled TotEZ normalized by the annual mean TotEZ provides a useful index of seasonal variability, which we denote as the Seasonal Flux Index (SFI). For BATS and NABE, annual values of the SFI are 2.5 and 2.1 respectively, indicating that much of the particle export occurs during bloom periods. Globally, SFI values are large (>2) poleward of 40° (Figure 6f). Overall, more than 25% of the latitude-longitude bins examined have an annual SFI range that exceeds the local mean value (>1), and 15.5% have variations that exceed twice that (Figure 7d).

4.4. Model Sensitivity

Model sensitivity is tested by serially perturbing either the model parameters or the input data selected. Estimates of the globally summed TotEZ and global mean values for TotEZ, the EZ-ratio, and AlgEZ/TotEZ from the perturbed case are compared with the baseline case (Table 1). It should be noted that evaluation of global summary statistics is only one way of understanding model sensitivity and similar global statistics could result from two trials with different spatial patterns.

The importance of the model parameter values was evaluated by serially varying their magnitudes by a factor of approximately 2 in a number of trials and evaluating resulting global summary statistics. A total of eight trials were performed to assess the role of the parameter choices. Large changes in the efficiency with which grazing on microphytoplankton creates flux (f_{FecM}) had a small influence on the global summary estimates (~10% difference from the baseline case; Table 1). Factor of 2 changes in the assumed f_{Alg} value had little influence on global averages of TotEZ or the EZ-ratio (again ~10% difference from the baseline case), although, as expected, the global mean value of AlgEZ/TotEZ was altered by nearly a factor of 2 (Table 1). Twofold changes in the assumed value of m_{ph} had a slightly larger influence on the global summary estimates (less than ~ 25%) compared with the factor of 2 alterations in either f_{FecM} or f_{Alg}.

The largest effects on the global averages of total carbon export and the EZ-ratio were found by varying values of f_{FecS}, the efficiency by which grazing on small phytoplankton creates a sinking particle flux (Table 1). Factor of 2 increases in f_{FecS} may not make much sense because small phytoplankton are grazed largely by microzooplankton as part of the microbial loop, and microzooplankton in turn need to be grazed by mesozooplankton to create a sinking fecal flux (Figure 1) [e.g., *Michaels and Silver*, 1988; *Boyd and Stevens*, 2002]. Hence, such large increases in f_{FecS} are unlikely, as there are many dissipative food-web processes

Table 1. Sensitivity Tests of Model Robustness to Parameter and Input Data Perturbation[a]

f_{FecM} (-)	f_{FecS} (-)	f_{Alg} (-)	m_{ph} (d^{-1})	Global TotEZ (Pg C yr^{-1})	(%)	AvTotEZ (mg C m^{-2} d^{-1})	(%)	AvEZRatio (-)	(%)	AvAlgRatio (-)	(%)
Baseline Parameters											
0.3	0.1	0.1	0.1	5.69	-	47.2	-	0.103	-	0.127	-
Parameter Perturbations											
0.4	0.1	0.1	0.1	6.21	9.1	52.0	10.2	0.112	8.7	0.116	−8.7
0.2	0.1	0.1	0.1	5.16	−9.3	42.5	−10.0	0.093	−9.7	0.141	11.0
0.3	0.05	0.1	0.1	4.00	−29.7	34.0	−28.0	0.073	−29.1	0.176	38.6
0.3	0.2	0.1	0.1	9.07	59.4	73.7	56.1	0.163	58.3	0.084	−33.6
0.3	0.1	0.2	0.1	6.20	9.0	51.9	10.0	0.113	9.7	0.225	77.2
0.3	0.1	0.05	0.1	5.43	−4.5	44.9	−4.9	0.098	−4.9	0.068	−46.5
0.3	0.1	0.1	0.2	4.52	−20.6	38.1	−19.3	0.077	−25.2	0.220	73.2
0.3	0.1	0.1	0.05	6.32	11.1	52.8	11.9	0.119	15.5	0.107	−15.7
Input Data Perturbations											
VGPM NPP algorithm				5.36	−5.8	49.2	4.2	0.099	−3.9	0.148	16.5
$P_T = f$(Chl) and fixed P_T/Chl				6.12	7.6	51.0	8.1	0.117	13.6	0.112	−11.8
F_{BVM} using $D_{max} = 100\ \mu m$				6.49	14.1	54.4	15.3	0.118	14.6	0.160	26.0
F_{BVM} using $D_{min} = 1\ \mu m$				5.98	5.1	49.6	5.1	0.108	4.8	0.148	16.5
F_{BVM} using $D_{spl} = 10\ \mu m$				6.86	20.6	57.4	21.6	0.124	20.4	0.182	43.3
F_{BVM} using $D_{spl} = 30\ \mu m$				4.97	−12.7	40.9	−13.3	0.089	−13.6	0.085	−33.1
Ensemble Mean and Standard Deviation											
				Global TotEZ (Pg C yr^{-1})		AvTotEZ (mg C m^{-2} d^{-1})		AvEZRatio (-)		AvAlgRatio (-)	
				5.89	1.17	49.3	9.3	0.107	0.022	0.140	0.047

[a]The (%) columns are percent deviation of the global summary statistics from the baseline case.

along this pathway if it is to create a sinking fecal flux. That said changes that increase the efficiency or shorten the path from small phytoplankton to export are more important for global summary statistics.

The choices of input data, such as the NPP algorithm, are tested in a similar manner where the input data product is switched and the global summary statistics are recalculated. Replacing the CbPMv2 NPP data product with the VGPM NPP product had a small (<6%) influence on global TotEZ or EZ-ratio values although larger influence (~17%) on the global mean AlgEZ/TotEZ ratio (Table 1). Estimating phytoplankton carbon from satellite-measured chlorophyll *a* concentrations and a fixed C/Chl ratio of 50 also had relatively small influences on global statistics (< 14%). Last, altering the assumptions used in partitioning the particle size spectra into microphytoplankton biovolumes had, for the most part, small influences on resulting global summary statistics. Differences are larger (15 to 21% for global TotEZ) if the boundaries in the definition of microphytoplankton are altered (changing either D_{max} or D_{spl}). In summary, the exact choice of data product used had a surprisingly small role in the resulting summary statistics.

The ensemble average of the 15 trials provides a global export value of 5.9 (1.2 SD) Pg C yr^{-1}. The uncertainty about the ensemble mean value is approximately 20% and accounts for a wide range uncertainties in parameter choices and input data assumptions. Similarly, the global mean EZ-ratio and AlgEZ/TotEZ ratio are 0.11 (0.02 SD) and 0.14 (0.05 SD), respectively. The relatively small variations about the ensemble means demonstrate the robustness of the present approach to reasonably large variations in model parameters and input data choices, and they provide a strong measure of confidence in the resulting global fluxes.

4.5. Interannual Variability in Global Carbon Export and its Efficiency

The present approach can be easily adapted to assess interannual variations in carbon fluxes. The time series of global anomalies of TotEZ from its climatological monthly mean is shown in Figure 8a. Data are used only equatorward of 50° latitude and only to the end of 2008 due to the lack of consistent coverage. Over the available record, global TotEZ anomalies, <TotEZ′>, vary by just over 0.5 Pg C yr^{-1}, roughly 10% of the climatological global integral. The biggest changes appear to be associated with the recovery from the 1997/1998 El Niño. No significant trends in < TotEZ′ > were found as a function of time over the available record.

The zonal variations contributing to the global TotEZ anomalies are shown in Figure 8b, where warm colors represent the positive contributions to the global anomaly and cool colors represent negative contributions. In general, the tropics and regions poleward of 35° latitude make the largest contributions to < TotEZ′>. Comparatively, the subtropical oceans make little contribution to global anomalies in TotEZ. Also apparent in

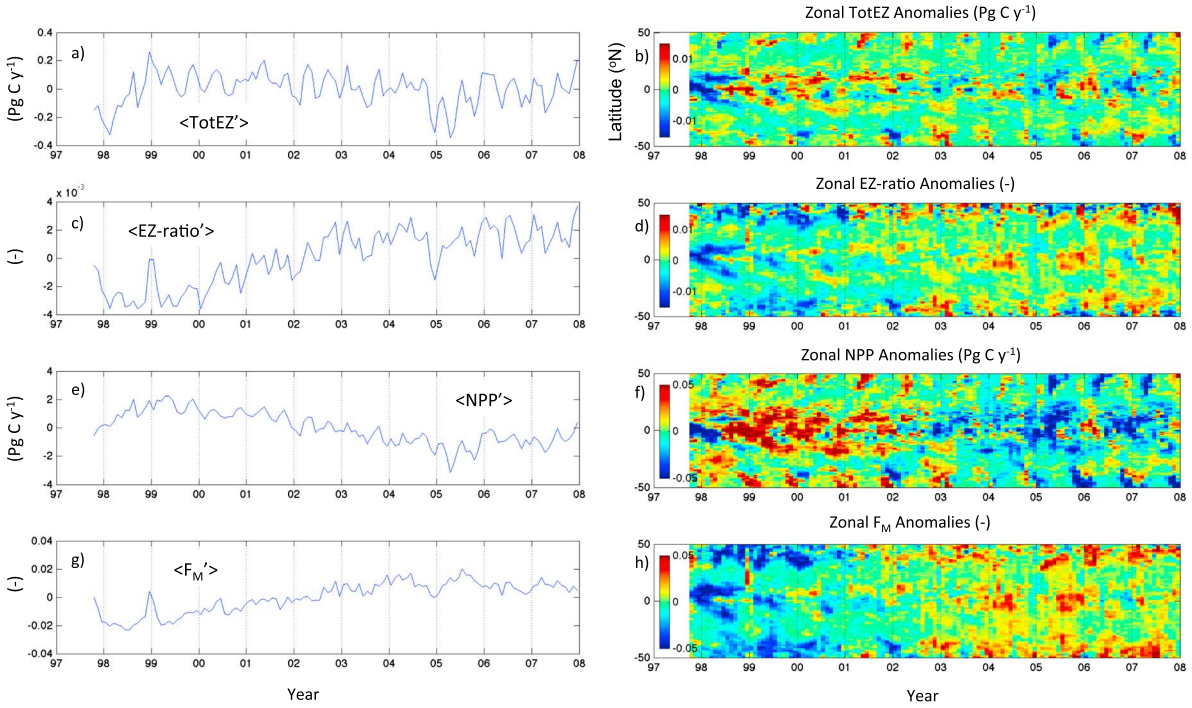

Figure 8. (left) Temporal changes in the global monthly anomalies for (a) $<$TotEZ'$>$, (c) $<$EZ-ratio'$>$, (e) $<$NPP'$>$, and (g) $<F_M'>$. (right) Temporal changes in the monthly anomalies for (b) $<$TotEZ'$>$, (d) $<$EZ-ratio'$>$, (f) $<$NPP'$>$, and (h) $<F_M'>$ summed (TotEZ and NPP) or averaged (EZ-ratio and F_M) over each zone of latitude. Data used are equatorward of 50° latitude to maximize coverage issues.

Figure 8b is the recovery from the 1997/1998 El Niño from low to high export and the propagation of these anomalies to higher latitudes as the 1999 La Niña forms in the tropics. Beyond these changes, the latitude bands where increased global TotEZ anomalies are found roughly balance those zonal bands where decreased contributions occur (Figure 8b).

Global anomalies in the EZ-ratio, $<$EZ-ratio'$>$, show a range of variability of ~0.7% (Figure 8c) about a mean value of 10.3%. Interestingly, a significantly increasing trend in $<$ EZ-ratio' $>$ is found (slope = 0.053% yr^{-1}; $r^2 = 0.67$; $p < 0.001$). The regions contributing to the changes in the global EZ-ratio anomaly are again localized in tropical and subarctic latitudes (Figure 8d).

The lack of a secular trend in global TotEZ anomalies while $<$ EZ-ratio' $>$ is increasing implies that global NPP anomalies must be declining over the observed period (Figure 8e). The global NPP anomalies, $<$NPP'$>$, do indeed show a linear decrease over time of -0.29 Pg C yr^{-1} ($r^2 = 0.58$; $p < 0.001$), consistent with previous analyses [e.g., *Behrenfeld et al*., 2006]. Much of the changes is found again in the tropics where initially largely positive NPP anomalies (with the exception of the 1997/1998 El Niño) become negative after 2003 (Figure 8f). Large changes are also seen in the higher latitudes but with a distinct seasonal pattern suggesting a change in the annual cycle.

The question now arises what is causing the increasing EZ-ratio. Global monthly anomalies of the fraction of microphytoplankton biovolume, $<F_M'>$, show an increasing trend in time (+0.30% yr^{-1}; $r^2 = 0.67$; $p < 0.001$; Figure 8g). Changes in zonal F_M anomalies are found primarily in the tropical and subarctic latitudes (Figure 8h). In particular, a strong correspondence is observed between the zonal patterns of F_M and EZ-ratio anomalies suggesting that changes in F_M are driving changes in the EZ-ratio anomalies (compare Figures 8d and 8h). In fact, recalculating the global and zonal anomalies for TotEZ and the EZ-ratio using the monthly climatology for F_M supports this assertion (Figure S4). Long-term changes in the global-averaged values of slope of the particle size spectrum and size-fractionated biovolumes have been noted previously from this data set [*Kostadinov et al*., 2010]. An examination of SeaWiFS clear-water remote-sensing radiance ratio anomalies suggest that the observed increases in $<F_M'>$ are not likely caused by unaccounted changes in the SeaWiFS calibration factors (B. Franz, personal communication, 2013).

5. Discussion

We have introduced a mechanistic approach for estimating the global carbon export from the euphotic zone using satellite observations and a food-web model. The model reproduces regional-scale TotEZ field observations, produces the expected global patterns of TotEZ and the EZ-ratio, and predicts a global total export of ~6 Pg C yr^{-1} with an uncertainty of ~20% about this mean value. Importantly, it reveals ecologically consistent global patterns in export and export efficiency that are not found in previous assessments. The model only has four parameters, each with a logical physical interpretation, and the resulting global flux summaries are only weakly dependent on the exact choice of parameters used or choice of input data used. The approach provides a diagnostic tool for addressing time and space variability of particle export and a frame to improve our understanding of the processes driving carbon export.

5.1. Paths to Improved Global Assessments of TotEZ and the EZ-Ratio

The food-web model (Figure 1) simulates particle export flux by accounting for the flows of net primary production (NPP) through microphytoplankton (P_M) and small phytoplankton (P_S). Hence, the present approach's fidelity is tightly tied to the ability to remotely observe NPP and the fraction of biomass in the microphytoplankton size class (F_M). The importance of these two parameters in the determination of TotEZ is seen in the lack of temporal trends of the global anomalies for TotEZ, $<$TotEZ$'>$, as decreases in $<$ NPP$' >$ are largely counteracted by increases in $< F_M' >$ (Figures 8a, 8e, and 8g). The dominant balance between NPP and grazing in the size-fractionated phytoplankton biomass balances (Figures 4 and S2) also illustrates the importance of NPP and F_M to the determination of TotEZ.

Clearly, improvements are needed for the remote-sensing proxies used. As is often the case in remote-sensing science, these improvements are tied to the availability of data to develop and validate satellite data algorithms. For some parameters such as phytoplankton carbon biomass or the slope of the particle size spectrum, globally distributed data are only now becoming available [e.g., *Buonassissi and Dierssen*, 2010; *Graff et al*., 2012; *Martinez-Vicente et al*., 2013]. Others, like NPP, have comparatively vast data sets (^{14}C incorporation observations) but are of mixed quality, and it remains an open question if ^{14}C incorporation actually measures NPP [e.g., *Peterson*, 1980; *Marra*, 2009]. Fortunately, the choice of data set used or the assumptions applied have surprisingly little influence on the modeled global statistics (section 4.4).

The framework of the food-web model is central to the model. The model itself is very simple (Figure 1) and assumes that the transformation fractions used to route primary production energy into flux components, f_{Alg}, f_{FecM}, and f_{FecS}, are globally fixed. Oceanic food webs are far more complicated. For example, impacts of gelatinous zooplankton on pelagic food webs will be different from that of a copepod or an euphausiid-dominated grazer community, and there are trophic classes other than herbivory and carnivory (i.e., mixotrophy, detritivory, coprophagy, etc.). As such, the present model should really be thought of only as a first step. The key improvements needed are to parameterize the transformation factors (cf., f_{Alg}, f_{FecM}, etc.) for changing plankton community composition. The challenge is that these parameterizations need to be functions of remotely sensible variables while having predictive power. The particle size distribution satellite data products used here are potentially useful for this purpose as should remote-sensing methodologies that quantify biomass in different phytoplankton functional types [e.g., *Alvain et al*., 2005; *Bracher et al*., 2009]. These improvements require data sets that span food-web dynamics to ocean optics observations.

Last, the end-to-end validation of the model performed here is clearly limited. The data sources were selected by *Buesseler and Boyd* [2009] based upon their ability to estimate TotEZ, the particle export flux at the base of the euphotic zone, and to span a range of conditions. Most available sediment trap or ^{234}Th flux observations are at fixed depths (100 or 150 m), which is often deeper than the optically determined euphotic zone depth (Figure 2a). Depth-resolved flux profiles are most commonly available from ^{234}Th disequilibrium profiles but also require knowledge of the ^{234}Th:POC ratio as a function of depth in order to calculate the flux at Z_{eu} [e.g., *Buesseler et al*., 2006]. Also, sediment traps or ^{234}Th only capture TotEZ over a short period of an evolving seasonal cycle (Figure 5c). The *Buesseler and Boyd* [2009] TotEZ data set was created by a limited number of research groups using similar protocols conducted as part of larger programs where ancillary biogeochemical information was readily available. Hence, the present results are likely more robust than had we combined different approaches and methods. Again this is an area where improved data sets aimed at addressing states of the biological pump would improve remote-sensing-based estimates of TotEZ.

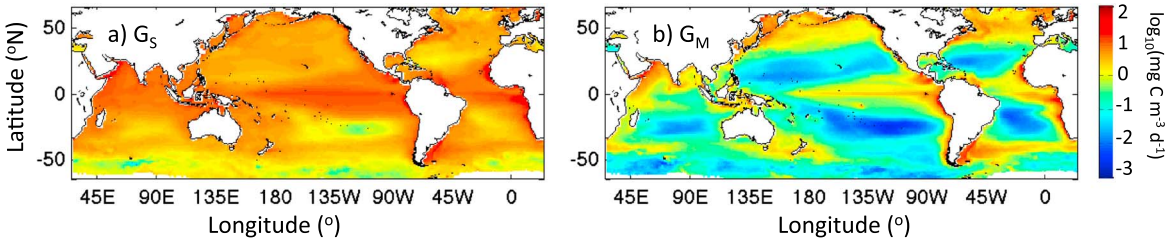

Figure 9. Global distributions of the annual mean grazing mortality for (a) small phytoplankton, G_S, and for (b) microphytoplankton, G_M. The values are $\log_{10}$-transformed and the same color scale is used for both plots.

5.2. Grazing Rate Estimates From Satellite Observations

Knowledge of zooplankton abundances and grazing rates on regional to global scales remains poorly known compared with pelagic phytoplankton stocks and rates [e.g., *Buitenhuis et al.*, 2006, 2013; *Stock and Dunne*, 2010; *Moriarty et al.*, 2013]. There are many reasons for this: inherently patchy distributions in space and time, difficulties in collecting vertically resolved profiles, tedious sample analyses, uncertainties in rate estimation protocols, vertical migration behaviors, complex and long-lived life cycles, etc. It seems unlikely that a satellite remote-sensing tool could be developed that would uniquely determine zooplankton abundances and rates. Hence, we are left to infer their influence by addressing phytoplankton dynamics.

The present modeling retrieves estimates of grazing mortality rates for large and small phytoplankton abundances, G_M and G_S, respectively. Annual mean distributions for G_M and G_S are shown in Figure 9. Mean values of G_M vary by more than 4 orders of magnitude over global scales while mean G_S values vary by less than 2 orders of magnitude. Interestingly, mean values of G_M and G_S are of comparable magnitude when values of G_M are at their highest (Figure 9). These regions coincide with the most productive oceanic regions (Figure 2e). Otherwise estimates of G_M are much smaller than G_S, especially in the oligotrophic ocean where these differences are greater by 2 orders of magnitude.

The results of the size-fractionated phytoplankton biomass budgeting (Figure 4) suggest that the grazing estimates on size-fractionated phytoplankton may have a semblance to reality. The dominant balance found in the surface layer biomass budget (equation (4)) was between the size-fractionated NPP and zooplankton grazing while the other terms were generally smaller by a factor of more than 5 (Figures 4 and S2). Hence, the magnitudes of the grazing rate estimates on size-fractionated phytoplankton are set largely by the observed NPP determinations and the assumptions used to partition microphytoplankton from smaller phytoplankton. The fidelity of both of these remote determinations was described previously and again stresses the importance of making improvements for these two satellite data products.

Last, it is important to recognize that the present approach quantifies the grazing mortality of microphytoplankton and small phytoplankton and not the grazing rates for mesozooplankton and microzooplankton. The simple food web (Figure 1) illustrates that mesozooplankton graze on both microphytoplankton and microzooplankton, while small zooplankton graze only on smaller phytoplankton. Even with this proviso, the upper-ocean biomass budgeting approach will likely provide a useful and unique tool for assessing modeled food webs in interdisciplinary ocean system models [e.g., *Buitenhuis et al.*, 2006; *Stock and Dunne*, 2010; *Sailley et al.*, 2013].

5.3. Quantifying the Ocean's Biological Pump From Satellite Observations

The present global estimates of TotEZ quantify the energy flows through phytoplankton into an aggregate and fecal sinking particle flux using an idealized food-web model. The present approach is unique in that it enables interannual changes in particle export and its efficiency to be assessed from remote-sensing data. However, export via sinking particles is one of several pathways where organic carbon is exported from the surface ocean. For example, the advection of dissolved organic carbon (DOC) from the surface ocean is not included. Recent estimates of the global DOC flux are ~2 Pg C yr^{-1} [*Hansell et al.*, 2009]. This global DOC flux combined with the present estimate of the sinking carbon export flux of ~6 Pg C yr^{-1} results in a total carbon export of ~8 Pg C yr^{-1}. A complete assessment of carbon export from the surface ocean must account for this and other additional pathways.

The model does account, at least partially, for the export of carbon from the surface ocean by migrating zooplankton [e.g., *Steinberg et al.*, 2000]. The upper layer biomass budgeting (equation (4)) accounts for the

total grazing losses of phytoplankton, assuming the other loss terms (direct algal flux, nongrazing biological losses, etc.) are well modeled or small. The grazing losses of mixed layer phytoplankton biomass are then routed into a sinking flux following equation (3). Although this approach accounts for export from zooplankton grazing, it does not partition this export into fecal particle sinking versus vertical migration and assumes that the fraction of grazed energy that is transformed into export is the same for the two pathways. Although carbon export by migrating zooplankton is included in some way in the modeling, it does point out limitations in the present approach.

Looking deeper into the food-web model, one should ask, "Well what exactly does the food-web model quantify?" In many ways, we are estimating the sinking particle flux under "typical" conditions given the fixed nature of the transformation factors that route food-web fluxes to export (Figure 1). The character of the input variables (cf., F_M, NPP, etc.) can alter the relative pathways that create export flux and this likely explains much of the robust nature of the approach for estimating global TotEZ values (Table 1). However, the structure and function of pelagic food webs are not fixed in time or in space. Extreme export fluxes can occur under "unusual" conditions when the biomass is dominated by a single component such as during a diatom or salp bloom [e.g., *Michaels and Silver*, 1988; *Boyd and Trull*, 2007]. Further, pelagic food webs have a wide range of trophic interactions beyond herbivory and carnivory, which are not included in the present model. The challenge is to create flexible food-web models that account accurately for the above alternatives while still being able to be applied using available observations. New methods for quantifying phytoplankton functional types or changes in the particle size spectrum provide some hope but the parameterization of the food-web processes with available observations is challenging. And again, these improvements are limited by the availability of high-quality data sets to parameterize the models.

Finally, the biological pump is more than just the export of carbon from the euphotic zone. Understanding the biological pump also requires the quantification of the vertical attenuation of the export flux below the euphotic zone as well [e.g., *Buesseler et al.*, 2007; *Dunne et al.*, 2007; *Boyd and Trull*, 2007; *Burd et al.*, 2010]. Multiple processes contribute to the attenuation of the vertical export flux to depth including zooplankton grazing, microbial degradation, organic carbon solubilization, vertical migration active transport, aggregate fragmentation and aggregation, etc. Information for many of the processes are available and provide paths for extending the modeling-observational data synthesis approach presented here to depth.

Acknowledgments

D.A.S. and K.O.B. acknowledge support from the National Aeronautics and Space Administration (NNX11AF63G). S.C.D. and S.F.S. acknowledge support from the National Science Foundation through the Center for Microbial Oceanography: Research and Education (C-MORE) (NSF EF-0424599). Computational assistance from Erik Fields is gratefully acknowledged.

References

Aksnes, D. L., and P. Wassmann (1993), Modeling the significance of zooplankton grazing for export production, *Limnol. Oceanogr.*, *38*, 978–985.

Alvain, S., C. Moulin, Y. Dandonneau, and F. M. Breon (2005), Remote sensing of phytoplankton groups in case 1 waters from global SeaWiFS imagery, *Deep Sea Res., Part I*, *52*, 1989–2004.

Aumont, O., and L. Bopp (2006), Globalizing results from ocean in situ iron fertilization studies, *Global Biogeochem. Cycles*, *20*GB2017, doi:10.1029/2005GB002591.

Banse, K. (1992), Grazing, temporal changes of phytoplankton concentrations, and the microbial loop in the open sea, in *Primary Productivity and Biogeochemical Cycles in the Sea*, edited by P. Falkowski and A. D. Woodhead, pp. 409–440, Plenum, New York.

Banse, K. (2013), Reflections about chance in my career, and on the top-down regulated world, *Annu. Rev. Mar. Sci.*, *5*, 1–19.

Behrenfeld, M. J. (2010), Abandoning Sverdrup's critical depth hypothesis on phytoplankton blooms, *Ecology*, *91*, 977–989.

Behrenfeld, M. J., and P. G. Falkowski (1997), Photosynthetic rates derived from satellite-based chlorophyll concentration, *Limnol. Oceanogr.*, *42*, 1–20.

Behrenfeld, M. J., E. Boss, D. A. Siegel, and D. M. Shea (2005), Carbon-based ocean productivity and phytoplankton physiology from space, *Global Biogeochem. Cycles*, *19*, GB1006, doi:10.1029/2004GB002299.

Behrenfeld, M. J., R. T. O_Malley, D. A. Siegel, C. R. McClain, J. L. Sarmiento, G. C. Feldman, A. J. Milligan, P. G. Falkowski, R. M. Letelier, and E. S. Boss (2006), Climate-driven trends in contemporary ocean productivity, *Nature*, *444*, 752–755.

Behrenfeld, M. J., S. C. Doney, I. Lima, E. S. Boss, and D. A. Siegel (2013), Annual cycles of ecological disturbance and recovery underlying the subarctic Atlantic spring plankton bloom, *Global Biogeochem. Cycles*, *27*, doi:10.1002/gbc.20050.

Billett, D. S. M., et al. (1983), Seasonal sedimentation of phytoplankton to the deep-sea benthos, *Nature*, *302*, 520–522.

Bopp, L., P. Monfray, O. Aumont, J.-L. Dufresne, H. Le Treut, G. Madec, L. Terray, and J. C. Orr (2001), Potential impact of climate change on marine export production, *Global Biogeochem. Cycles*, *15*, 81–99, doi:10.1029/1999GB001256.

Boyd, P., and P. Newton (1997), Measuring biogenic carbon flux in the ocean, *Science*, *275*, 554.

Boyd, P. W., and C. L. Stevens (2002), Modelling particle transformations and the downward organic carbon flux in the NE Atlantic Ocean, *Prog. Oceanogr.*, *52*, 1–29.

Boyd, P. W., and T. W. Trull (2007), Understanding the export of marine biogenic particles: Is there consensus?, *Prog. Oceanogr.*, *72*, 276–312.

Boyd, P. W., M. P. Gall, M. W. Silver, S. L. Coale, R. R. Bidigare, and J. L. K. Bishop (2008), Quantifying the surface-subsurface biogeochemical coupling during the VERTIGO ALOHA and K2 studies, *Deep Sea Res., Part II*, *55*, 1578–1593.

Bracher, A., M. Vountas, T. Dinter, J. P. Burrows, R. Röttgers, and I. Peeken (2009), Quantitative observation of cyanobacteria and diatoms from space using PhytoDOAS on SCIAMACHY data, *Biogeosciences*, *6*, 751–764.

Buesseler, K. O., and P. W. Boyd (2009), Shedding light on processes that control particle export and flux attenuation in the twilight zone of the open ocean, *Limnol. Oceanogr.*, *54*, 1210–1232.
Buesseler, K. O., et al. (2006), An assessment of particulate organic carbon to thorium-234 ratios in the ocean and their impact on the application of ^{234}Th as a POC flux proxy, *Mar. Chem.*, *100*, 213–233.
Buesseler, K. O., et al. (2007), Revisiting carbon flux through the ocean's twilight zone, *Science*, *316*, 567–570.
Buitenhuis, E. T., C. Le Quéré, O. Aumont, G. Beaugrand, A. Bunker, A. Hirst, T. Ikeda, T. O'Brien, S. Piontkovski, and D. Straile (2006), Biogeochemical fluxes through mesozooplankton, *Global Biogeochem. Cycles*, *20*, GB2003, doi:10.1029/2005GB002511.
Buitenhuis, E. T., et al. (2013), MAREDAT: Towards a world atlas of Marine Ecosystem Data, *Earth Syst. Sci. Data*, *5*, 227–239.
Buonassissi, C. J., and H. M. Dierssen (2010), A regional comparison of particle size distributions and the power law approximation in oceanic and estuarine surface waters, *J. Geophys. Res.*, *115*, C10028, doi:10.1029/2010JC006256.
Burd, A. B., et al. (2010), Assessing the apparent imbalance between geochemical and biochemical indicators of meso- and bathypelagic biological activity: What the @$#! is wrong with present calculations of carbon budgets?, *Deep Sea Res., Part II*, *57*, 1429–1592.
de Boyer Montégut, C., G. Madec, A. S. Fischer, A. Lazar, and D. Iudicone (2004), Mixed layer depth over the global ocean: An examination of profile data and a profile-based climatology, *J. Geophys. Res.*, *109*, C12003, doi:10.1029/2004JC002378.
DeVries, T., F. Primeau, and C. Deutsch (2012), The sequestration efficiency of the biological pump, *Geophys. Res. Lett.*, *39*, L13601, doi:10.1029/2012GL051963.
Doney, S. C., I. Lima, J. K. Moore, K. Lindsay, M. J. Behrenfeld, T. K. Westberry, N. Mahowald, D. M. Glover, and T. Takahashi (2009), Skill metrics for confronting global upper ocean ecosystem-biogeochemistry models against field and remote sensing data, *J. Mar. Syst.*, *76*, 95–112.
Dunne, J. P., R. A. Armstrong, A. Gnanadesikan, and J. L. Sarmiento (2005), Empirical and mechanistic models for the particle export ratio, *Global Biogeochem. Cycles*, *19*, GB4026, doi:10.1029/2004GB002390.
Dunne, J. P., J. L. Sarmiento, and A. Gnanadesikan (2007), A synthesis of global particle export from the surface ocean and cycling through the ocean interior and on the seafloor, *Global Biogeochem. Cycles*, *20*, doi:10.1029/2006GB002907.
Evans, G. T., and J. S. Parslow (1985), A model of annual plankton cycles, *Biol. Oceanogr.*, *3*, 327–347.
Falkowski, P. G., R. T. Barber, and V. Smetacek (1998), Biogeochemical controls and feedbacks on ocean primary production, *Science*, *281*, 200–206.
Gehlen, M., L. Bopp, N. Emprin, O. Aumont, C. Heinze, and O. Ragueneau (2006), Reconciling surface ocean productivity, export fluxes and sediment composition in a global biogeochemical ocean model, *Biogeosciences*, *3*, 521–537.
Graff, J. R., A. J. Milligan, and M. J. Behrenfeld (2012), The measurement of phytoplankton biomass using flow-cytometric sorting and elemental analysis of carbon, *Limnol. Oceanogr. Methods*, *10*, 910–920.
Hansell, D. A., C. A. Carlson, D. J. Repeta, and R. Schlitzer (2009), Dissolved organic matter in the ocean: New insights stimulated by a controversy, *Oceanography*, *22*, 52–61.
Henson, S. A., R. Sanders, E. Madsen, P. J. Morris, F. Le Moigne, and G. D. Quartly (2011), A reduced estimate of the strength of the ocean's biological carbon pump, *Geophys. Res. Lett.*, *38*, L04606, doi:10.1029/2011GL046735.
Kostadinov, T. S., D. A. Siegel, and S. Maritorena (2009), Retrieval of the particle size distribution from satellite ocean color observations, *J. Geophys. Res.*, *114*, C09015, doi:10.1029/2009JC005303.
Kostadinov, T. S., D. A. Siegel, and S. Maritorena (2010), Global variability of phytoplankton functional types from space: Assessment via the particle size distribution, *Biogeosciences*, *7*, 3239–3257.
Kwon, E. Y., F. Primeau, and J. L. Sarmiento (2009), The impact of remineralization depth on the air–sea carbon balance, *Nat. Geosci.*, *2*, 630–635.
Lampitt, R. S., B. Boorman, L. Browna, M. Lucas, I. Salter, R. Sanders, K. Saw, S. Seeyave, S. J. Thomalla, and R. Turnewitsch (2008), Particle export from the euphotic zone: Estimates using a novel drifting sediment trap, ^{234}Th and new production, *Deep Sea Res., Part I*, *55*, 1484–1502.
Lampitt, R. S., I. Salter, B. A. de Cuevas, S. Hartman, K. E. Larkin, and C. A. Pebody (2010), Long-term variability of downward particle flux in the deep northeast Atlantic: Causes and trends, *Deep Sea Res., Part II*, *57*, 1346–1361.
Laws, E. A., P. G. Falkowski, W. O. Smith, H. Ducklow, and J. J. McCarthy (2000), Temperature effects on export production in the open ocean, *Global Biogeochem. Cycles*, *14*, 1231–1246.
Lutz, M. J., K. Caldeira, R. B. Dunbar, and M. J. Behrenfeld (2007), Seasonal rhythms of net primary production and particulate organic carbon flux to depth describe the efficiency of biological pump in the global ocean, *J. Geophys. Res.*, *112*, C10011, doi:10.1029/2006JC003706.
Marra, J. (2009), Net and gross productivity: Weighing in with ^{14}C, *Aquat. Microb. Ecol.*, *56*, 123–131.
Martinez-Vicente, V., G. Dall'Olmo, G. Tarran, E. Boss, and S. Sathyendranath (2013), Optical backscattering is correlated with phytoplankton carbon across the Atlantic Ocean, *Geophys. Res. Lett.*, *40*, 1154–1158, doi:10.1002/grl.50252.
McClain, C. R. (2009), A decade of satellite ocean color observations, *Annu. Rev. Mar. Sci.*, *1*, 19–42.
Michaels, A. F., and M. W. Silver (1988), Primary production, sinking fluxes and the microbial food web, *Deep-Sea Res.*, *35*, 473–490.
Morel, A., Y. Huot, B. Gentili, P. Werdell, S. Hooker, and B. Franz (2007), Examining the consistency of products derived from various ocean color sensors in open ocean (Case 1) waters in the perspective of a multi-sensor approach, *Remote Sens. Environ.*, *111*, 69–88.
Moriarty, R., E. T. Buitenhuis, C. Le Quéré, and M.-P. Gosselin (2013), Distribution of known macrozooplankton abundance and biomass in the global ocean, *Earth Syst. Sci. Data*, *5*, 241–257, doi:10.5194/essd-5-241-2013.
Peterson, B. J. (1980), Aquatic primary productivity and the ^{14}C-CO_2 method: A history of the productivity problem, *Annu. Rev. Ecol. Sys.*, *11*, 359–385.
Rutgers van der Loeff, M., et al. (2006), A review of present techniques and methodological advances in analyzing 234Th in aquatic systems, *Mar. Chem.*, *100*, 190–212.
Sailley, S. F., M. Vogt, S. C. Doney, M. N. Aita, L. Bopp, E. T. Buitenhuis, T. Hashioka, I. Lima, C. Le Quéré, and Y. Yamanaka (2013), Comparing food web structures and dynamics across a suite of global marine ecosystem models, *Ecol. Modell.*, *261*, 43–57.
Siegel, D. A., et al. (2001), The Bermuda BioOptics Project: Bio-optical modeling of primary production from space-sensible variables, *Deep Sea Res., Part II*, *48*, 1865–1896.
Siegel, D. A., et al. (2013), Regional to global assessments of phytoplankton dynamics from the SeaWiFS mission, *Remote Sens. Environ.*, *135*, 77–91.
Steinberg, D. K., C. A. Carlson, N. R. Bates, S. A. Goldthwait, L. P. Madin, and A. F. Michaels (2000), Zooplankton vertical migration and the active transport of dissolved organic and inorganic carbon in the Sargasso Sea, *Deep Sea Res., Part I*, *47*, 137–158.
Steinberg, D. K., C. A. Carlson, N. R. Bates, R. J. Johnson, A. F. Michaels, and A. H. Knap (2001), Overview of the US JGOFS Bermuda Atlantic Time-series Study (BATS): A decade-scale look at ocean biology and biogeochemistry, *Deep Sea Res., Part II*, *48*, 1405–1447.
Stock, C. A., and J. P. Dunne (2010), Controls on the ratio of mesozooplankton production to primary production in marine ecosystems, *Deep Sea Res., Part I*, *57*, 95–112.
Waples, J. T., C. Benitez-Nelson, N. Savoye, M. Rutgers van der Loeff, M. Baskaran, and Ö. Gustafsson (2006), An introduction to the application and future use of ^{234}Th in aquatic systems, *Mar. Chem.*, *100*, 166–189.
Westberry, T. K., M. J. Behrenfeld, D. A. Siegel, and E. Boss (2008), Carbon-based primary productivity modeling with vertically resolved photoacclimation, *Global Biogeochem. Cycles*, *22*, GB2024, doi:10.1029/2007GB003078.